J. Am. Soc. Mass Spectrom. (2013) 24:1641–1653
DOI: 10.1007/s13361-013-0630-0

FOCUS: ELECTRON TRANSFER DISSOCIATION: RESEARCH ARTICLE

Electron Transfer Dissociation of Photolabeled Peptides. Backbone Cleavages Compete with Diazirine Ring Rearrangements

Aleš Marek, Robert Pepin, Bo Peng, Kenneth J. Laszlo, Matthew F. Bush, František Tureček

Department of Chemistry, Bagley Hall, University of Washington, Seattle, WA, USA

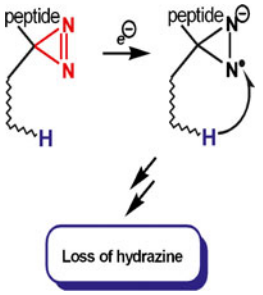

Abstract. Gas-phase conformations and electron transfer dissociations of pentapeptide ions containing the photo-Leu residue (L*) were studied. Exhaustive conformational search including molecular dynamics force-field, semi-empirical, ab initio, and density functional theory calculations established that the photo-Leu residue did not alter the gas-phase conformations of $(GL^*GGK + 2H)^{2+}$ and $(GL^*GGK\text{-}NH_2+H)^+$ ions, which showed the same conformer energy ranking as the unmodified Leu-containing ions. This finding is significant in that it simplifies conformational analysis of photo-labeled peptide ions. Electron transfer dissociation mass spectra of $(GL^*GGK + 2H)^{2+}$, $(GL^*GGK\text{-}NH_2+2H)^{2+}$,$(GL^*GGKK+2H)^{2+}$, $(GL^*GLK+2H)^{2+}$, and $(GL^*LGK+2H)^{2+}$ showed 16 %–21 % fragment ions originating by radical rearrangements and cleavages in the diazirine ring. These side-chain dissociations resulted in eliminations of N_2H_3, N_2H_4, $[N_2H_5]$, and $[NH_4O]$ neutral fragments and were particularly abundant in long-lived charge-reduced cation-radicals. Deuterium labeling established that the neutral hydrazine molecules mainly contained two exchangeable and two nonexchangeable hydrogen atoms from the peptide and underwent further H/D exchange in an ion–molecule complex. Electron structure calculations on the charge-reduced ions indicated that the unpaired electron was delocalized between the diazirine and amide π* electronic systems in the low electronic states of the cation-radicals. The diazirine moiety in $GL^*GGK\text{-}NH_2$was calculated to have an intrinsic electron affinity of 1.5 eV, which was further increased by the Coulomb effect of the peptide positive charge. Mechanisms are proposed for the unusual elimination of hydrazine from the photo-labeled peptide ions.

Key words: Electron transfer dissociation, Diazirine-labeled peptides, Radical dissociations

Received: 28 December 2012/Revised: 25 March 2013/Accepted: 25 March 2013/Published online: 30 April 2013

Introduction

Electron capture and transfer dissociations (ExD) of modified peptides have been of keen interest in the pursuit of elucidating the gas-phase chemistry of peptide radicals and cation radicals. Fixed-charge groups [1–10], radical traps [11–14], and backbone modifications [15–19] have been shown to have various, often very dramatic, effects on peptide ion fragmentation following electron attachment. In a distinct field of study, photochemically active labels have been used to study noncovalent protein–protein and protein–ligand interactions [20]. In particular, peptides and proteins incorporating the diazirine group have been used for photoinduced protein footprinting [21–23]. The diazirine ring absorbs light in the near UV region (340–360 nm) and undergoes facile ring opening and loss of N_2 to form a highly reactive carbene intermediate that can undergo insertion into covalent X–H bonds [24, 25]. In contrast to photochemical studies, the radical chemistry of diazirines has not been studied in detail in solution [26, 27] and, to our knowledge, there have been no studies of diazirine-containing peptide ions in the gas phase. In the context of our ongoing studies of gas-phase stapling and conformational properties of peptide ions [28], we investigated the methods for sequencing diazirine-modified peptide ions

Electronic supplementary material The online version of this article (doi:10.1007/s13361-013-0630-0) contains supplementary material, which is available to authorized users.

Correspondence to: František Tureček; *e-mail:* turecek@chem.washington.edu

using electron transfer dissociation (ETD) [29]. This revealed some unusual and novel rearrangements of diazirine-labeled peptide ions that competed with standard ETD backbone dissociations. Here we report the results of experimental and computational investigations aimed at elucidating the mechanisms of the newly discovered reactions.

Experimental

Materials

Peptides GLGGK, GLGGK-NH_2, GLGGKK, and photo leucine analogous GL*GGK, GL*GGK-NH_2, GL*GGKK, GL*GLK, and GL*LGK, where L* stands for the L-2-amino-4,4-azi-pentanoic acid residue (Pierce Biotechnology, Rockford, IL, USA), were synthesized on Wang resin (Bachem Americas, Torrance, CA, USA and Chem-Impex International, Wood Dale, IL, USA) using the Fmoc methodology according to literature procedures [30]. Fmoc protected photo leucine (L-2-amino-4,4-azi-pentanoic acid) was prepared according to the literature [31]. The other chemicals were purchased from Sigma-Aldrich (Saint Louis, MO, USA).

Methods

Peptide solutions (5–10 μM) in 50/50/1 water/methanol/acetic acid were electrosprayed to form precursor cations for ETD. Electrospray ionization of the Lys-containing pentapeptides produced both doubly protonated $(M + 2H)^{2+}$ and singly protonated $(M + H)^{+}$ ions, typically in a ~2:1 ratio. H/D exchange was accomplished by dissolving the peptides in 1:1 D_2O CH_3OD (99.5 %D) that contained 0.5 % CD_3COOD to achieve 7–10 μM concentrations and allowing the solutions to stand for several hours, typically overnight, in tightly capped vials. The peptide solutions were infused with a syringe pump into an open electrospray source consisting of a pulled fused silica capillary as the ESI needle that was positioned 2 mm from the orifice of the source transfer capillary. Simultaneously with electrospraying the D_2O/CH_3OD peptide solutions, a stream of nitrogen that was saturated with D_2O vapor at 20 °C was blown over the orifice and tip of the ESI needle from a 20-mm bore glass tubing that was brought within 2 mm of the ESI tip to cover the space the droplets travel to the vacuum system. Electron transfer dissociation mass spectra were measured on a Thermo Fisher Scientific (San Jose, CA, USA) LTQ XL linear ion trap instrument outfitted with a chemical ionization source for the production of fluoranthene anion radicals as ETD reagent. Precursor cations $(M + 2H)^{2+}$ were mass isolated with a window of 1.0 *m/z* unit and allowed to react for 100, 200, 300, and 500 ms with fluoranthene anions. The 200 ms ETD spectra are reported. Collision-induced dissociation of ETD-produced ions (MS^3) were run at a 30 ms excitation time and amplitudes achieving >60 % dissociation of the precursor ion. Another set of ETD mass spectra was obtained on a Waters (Manchester, UK) Synapt G2 tandem mass spectrometer furnished with an atmospheric pressure discharge ion source for the generation of negative reagent ions. Azulene was used as the negative CI reagent [32]. High resolution ETD mass spectra were obtained on a Thermo Fisher Scientific Orbitrap LTQ Velos instrument under the same conditions as used for the LTQ XL linear ion trap measurements. The resolving power was set at 60,000 or 100,000, as needed to resolve peak doublets. The exact fragment *m/z* values were calibrated internally on the known *m/z* of the $(M + 2H)^{2+}$ and $(M + H)^{+}$ ions.

Calculations

Conformational search was performed for $(GK+H)^{+}$, $(GLGGK\text{-}NH_2+H)^{+}$, and $(GLGGK + 2H)^{2+}$ using a home-built search engine, as described previously [33]. Briefly, 800,000 ion conformers of each $(GK+H)^{+}$ and $(GLGGK\text{-}NH_2+H)^{+}$ protonated at the Lys amino group, and $(GLGGK + 2H)^{2+}$ conformers protonated at the Lys and N-terminal amino groups were generated by replica-exchange molecular dynamics trajectory runs at 300–800 K, and 1000 structures of each group that were selected at regular intervals from each replica run were energy-sorted by PM6 full geometry optimization [34]. Eight thousand conformers for each peptide ion were grouped according to their hydrogen bonding patterns, and 200 lowest-energy conformers were ranked by single-point B3LYP/6-31+G(d,p) calculations. The ab initio and density functional theory calculations used the Gaussian 09 suite of programs [35]. Redundant replicates were compacted, and thirty five lowest-energy structures spanning a 20 kJ mol^{-1} energy interval were fully optimized by B3LYP [36, 37] and M06-2X [38] with the 6-31+G(d,p) basis set. Local energy minima were confirmed by frequency calculations. Scaled harmonic frequencies (0.963 for B3LYP calculations) along with moments of inertia were used to calculate 298 K enthalpies and entropies. Single-point calculations were performed for selected lowest-energy structures within a 20 kJ mol^{-1} energy interval. The single-point calculations used B3LYP, M06-2X, and MP2 (frozen core) [39] with the 6-311++G(2d,p) basis set. Three lowest-energy $(GLGGK\text{-}NH_2+H)^{+}$ conformers and two lowest-energy $(GLGGK + 2H)^{2+}$ conformers from the single-point calculations were modified using PCModel 9.2 (Serena Software, Riverside, CA, USA) to replace a Leu methyl group with a diazirine ring, and the new structures, $(GL*GGK\text{-}NH_2+H)^{+}$ and $(GL*GGK + 2H)^{2+}$, containing the photo leucine residue (L*) were fully reoptimized with B3LYP and M06-2X/6-31+G(d,p). The optimized ions were further characterized by frequency and single-point energy calculations.

Calculations of cation-radicals started with the optimized dication structures which were re-optimized with the charge-reduced electronic configuration at the spin-unrestricted UB3LYP/6-31+G(d,p) and UM06-2X/6-31+G(d,p) levels,

and the structures were confirmed as local energy minima or first-order saddle points by harmonic frequency calculations. Transition state searches were performed by step-wise mapping of the relevant parts of the potential energy surface followed by gradient optimizations to the first-order saddle point. The UB3LYP/6-31+G(d,p) and UM06-2X/6-31+G(d,p) searches were run independently to avoid false TS structures. Single point energies were calculated with UB3LYP/6-311++G(2d,p), UM06-2X/6-311++G(2d,p), and spin-projected PMP2(frozen core)/6-311++G(2d,p). The B3LYP and PMP2 energies were averaged to provide improved relative energies for cation-radicals [40–42]. Time dependent density functional theory (TD-DFT) [43] with the B3LYP and M06-2X functionals and the 6-311++G(2d,p) basis set was used to calculate the first 15 excited states of the vertically formed cation-radical configurations. Atomic charges and spin densities were calculated using the Natural Population Analysis formalism [44].

Results

ETD-MS^2 and ETD-CID-MS^3 Spectra

We first describe the ETD mass spectra of peptide ions derived from GLGGK, GLGGK-NH_2, and GLGGKK as well as their photoleucine analogues GL*GGK, GL*GGK-NH_2, GL*GGKK, and GL*GGKK-NH_2. Then we focus on a more detailed investigation of photoleucine containing peptides GL*GLK and GL*LGK. ETD of $(GLGGK + 2H)^{2+}$ ions (*m/z* 216, Figure 1a) gave a standard fragmentation pattern consisting of the charge-reduced $(M + H)^+$ ion at *m/z* 431, backbone fragments $\boldsymbol{c_4}$ (*m/z* 302), $\boldsymbol{z_3}$ (*m/z* 245), $\boldsymbol{z_2}$ (*m/z* 188), and $\boldsymbol{y_1}$ (*m/z* 147), and fragments due to loss of ammonia (*m/z* 415) followed by loss of C_3H_7 (*m/z* 372), C_4H_8 (*m/z* 359), and CO_2 (*m/z* 315). These are common cascade dissociations of peptide cation-radicals affecting the Leu side chain and the C-terminal carboxyl group [45–48]. The ETD spectrum of $(GL*GGK + 2H)^{2+}$ ions (*m/z* 222, Figure 1b) also showed backbone fragments $\boldsymbol{c_4}$ (*m/z* 314), $\boldsymbol{z_3}$ (*m/z* 245), $\boldsymbol{z_2}$ (*m/z* 188), $\boldsymbol{y_3}$ (*m/z* 261), $\boldsymbol{y_2}$ (*m/z* 204), and $\boldsymbol{y_1}$ (*m/z* 147). In addition, there was a prominent group of fragment ions at *m/z* 410–415 amounting to 17 % of ETD fragment ion intensities that were absent in the spectrum of $(GLGGK + 2H)^{2+}$. Accurate mass measurements identified these as *m/z* 415.2303 (loss of N_2H), *m/z* 413.2141 (loss of N_2H_3), *m/z* 412.2066 (loss of N_2H_4), *m/z* 411.1986 (loss of $[N_2H_5]$), and *m/z* 410.2147 (loss of $[NH_4O]$). The measured *m/z* values were within 0.0003 m.u. of the theoretical values and left no doubt about the elemental composition of the neutral losses. The ETD spectrum of $(GL*GGK + 2H)^{2+}$ ions, obtained by electron transfer from azulene anion-radicals in merged ion beams on the Synapt G2 instrument (Figure S1, Supplementary Data), also showed *m/z* 410–415 ions of correct exact masses, confirming that these fragmentations were not confined to a particular electron donor or the experimental conditions in the ion trap.

Very similar patterns of neutral losses were obtained for ETD of $(GL*GGK\text{-}NH_2+2H)^{2+}$, $(GL*GGKK+2H)^{2+}$, $(GL*GGKK\text{-}NH_2+2H)^{2+}$ (Figure S2, Supplementary Data), $(GL*GLK+2H)^{2+}$, and $(GL*LGK+2H)^{2+}$ (Figure 2a, b), but not for their analogues lacking the photoleucine residue. This indicated that the observed neutral losses were due to dissociations involving the diazirine ring. The ETD spectrum of $(GL*LGK+2H)^{2+}$ (Figure 2b) showed a higher relative intensity of the fragment ion at *m/z* 466 by loss of $[NH_4O]$. An additional feature was that the loss of N_2H_4 was accompanied by a minor loss of $[CH_3NH_3]$ that gave a baseline resolved doublet at *m/z* 468.2690 and 468.2565, respectively. Note that $[N_2H_5]$, $[CH_3NH_3]$, and $[NH_4O]$ are not stable molecules and so these neutral losses likely involve at least two neutral fragments.

The potential intermediates for these unusual neutral losses, $(M + H)^+$ and $(M+2H - NH_3)^+$, were investigated by CID-MS^3 experiments as illustrated for GL*GLK (Figure S3a, b, Supplementary Data). All fragments in the CID-MS^3 spectra were identified by exact mass measurements that showed match with the theoretical values within 0.0003 m.u. CID of the $(M+2H - NH_3)^+$ ions from GL*GLK and GL*LGK (Figure S3a, Supplementary Data) mainly gave fragment ions at *m/z* 455, 440, 427, and 412 due to side-chain losses of C_3H_7 and C_4H_8 in combination with elimination of N_2, as established from high-resolution MS^3 spectra. CID of the $(M + H)^+$ fragment ion at *m/z* 499 showed a dominant loss of N_2, while the *m/z* 466–470 fragments were absent (Figure S3b Supplementary Data). The same result was obtained for CID of the $(M + H)^+$ ion that was generated by electrospray ionization of the peptide and likewise for the $(M + H)^+$ ions from GL*LGK. The *m/z* 466 and *m/z* 468 fragments were minor and could be accounted for by the residual isotope satellites of the *m/z* 465 and 467 fragment ions. These experiments unambiguously established that the losses of N_2H_x and $[NH_4O]$ occurred directly from the charge-reduced $(M + 2H)^{+\cdot}$ cation-radicals and not by secondary dissociations of stable intermediates.

The fragment ions formed by the unusual losses of N_2H_x and $[NH_4O]$ were further studied by CID-MS^3 experiments. Figure S4a,b in Supplementary Data shows the CID-MS^3 spectra of the *m/z* 468 fragment ions from ETD of the respective GL*GLK and GL*LGK ions. The Figure S4a in Supplementary Data spectrum shows amide backbone cleavages between the L-K ($\boldsymbol{y_1}$ and $\boldsymbol{b_4}$), G-L ($\boldsymbol{b_3}$), and G-(L*-N_2H_4) ($\boldsymbol{y_4}$) residues, but not between the (L*-N_2H_4)-G residues. The *m/z* 451 fragment ion (*m/z* 451.2303) indicates a loss of CH_5 from the precursor cation-radical. As CH_5 is not a stable molecule, its loss must occur in two steps. Noteworthy is the lack of N–C_α bond dissociations in the CID-MS^3 spectrum in Figure S4a Supplementary Data.

The Figure S4b Supplementary Data spectrum showed a dominant elimination of C_4H_8 from the *m/z* 468 precursor cation-radical forming the strong *m/z* 412 fragment ion. The elimination of C_4H_8 is a radical driven dissociation that undoubtedly occurs from the Leu side chain and requires

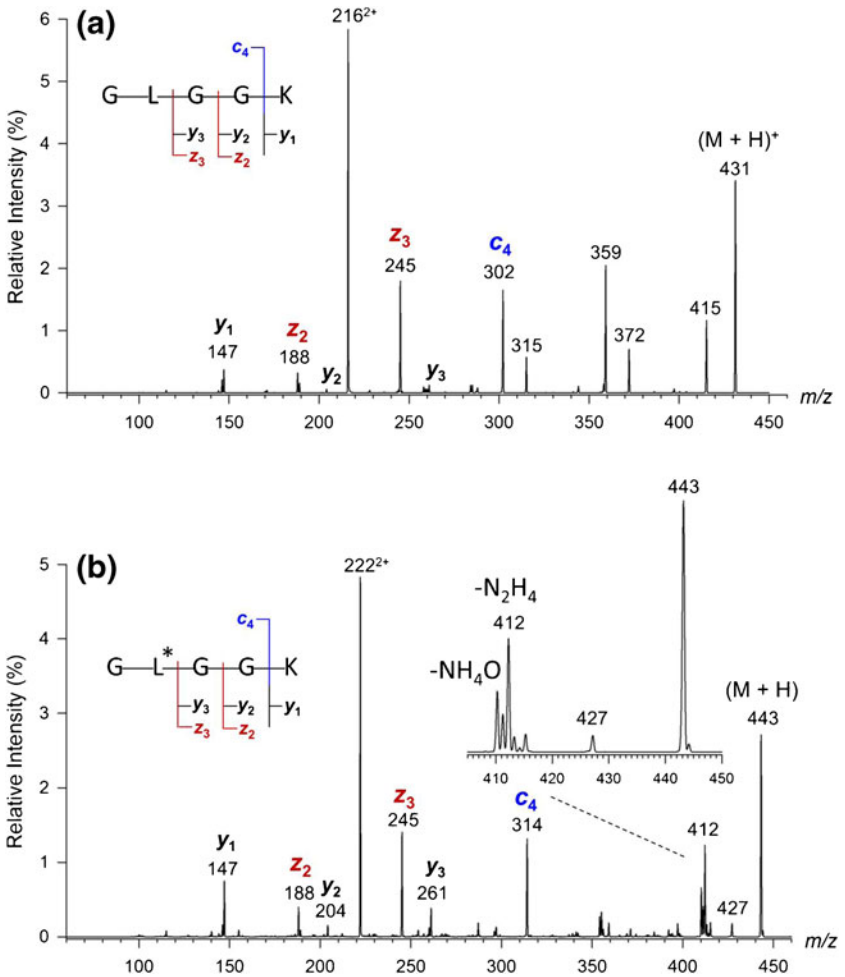

Figure 1. Electron transfer dissociation mass spectra of **(a)** $(GLGGK + 2H)^{2+}$ and **(b)** $(GL^*GGK + 2H)^{2+}$

abstraction of the γ-hydrogen atom by a sterically accessible acceptor [47, 48]. Note that the *m/z* 412 fragment ion in the Figure S4a spectrum (*m/z* 412.2559) is formed by elimination of C_2H_2NO from the N-terminal Gly residue, not C_4H_8 form the remote Leu side chain. A minor z_3 fragment (*m/z* 301) and the related $z_3 - C_3H_7$ (*m/z* 258) indicated N–C_α backbone cleavage between the $(L^*\text{-}N_2H_4)$-L residues in the Figure S4b spectrum. In addition, the Figure S4b spectrum showed backbone amide cleavages giving the y_1, b_4, b_3, and related b_4+H_2O and a_3 fragment ions. These fragments are likely to be formed by proton-driven dissociations without necessary participation of the radical centers. Hence, the dissociations of the isomeric *m/z* 468 cation-radicals show competitive radical and charge driven dissociations. Interesting is the predominance of N-terminal *b* fragments that preserved the charging proton in competition with the C-terminal Lys residue.

The CID-MS^3 spectra of the even-electron *m/z* 466 fragment ions from ETD of the respective GL*GLK and GL*LGK ions showed dominant elimination of water and backbone amide cleavages between the L-K or G-K and G-L or L-G residues. No cleavages between the G-$(L^*\text{-}NH_4O)$ and $(L^*\text{-}NH_4O)$-G or $(L^*\text{-}NH_4O)$-L residues were observed (Figure S5a,b, Supplementary Data).

Lifetime Effects on Cation-Radical Dissociations

A closer inspection of the ETD spectra of $(GL^*GLK+2H)^{2+}$ and $(GL^*LGK+2H)^{2+}$ revealed that they contained minor surviving charge-reduced cation-radicals at *m/z* 500.3065 that were distinguished from the residual ^{13}C and ^{15}N isotope satellites of the more abundant $(M + H)^+$ ions at *m/z* 500.3020 and 500.2957, respectively. The long-lived $(GL^*LGK+2H)^{+\cdot}$ cation-radical, which was not contaminated with $^{13}C+^{15}N$ isotope satellites, was selected by mass and its CID showed exclusive losses of N_2H_4 and $[NH_4O]$ with an intensity ratio that was very similar to that in the ETD spectrum of $(GL^*LGK+2H)^{2+}$ shown in Figure 2b.

The properties of gas-phase peptide ions can be modified by complexation with crown ethers [49]. We used this technique to generate long-lived $(GL^*GLK+2H)^{+\cdot}$ cation-radicals according to two alternative dissociation-isolation sequences. Both used electrospray of GL*GLK with 18-crown-6-ether (CE) which gave abundant noncovalent

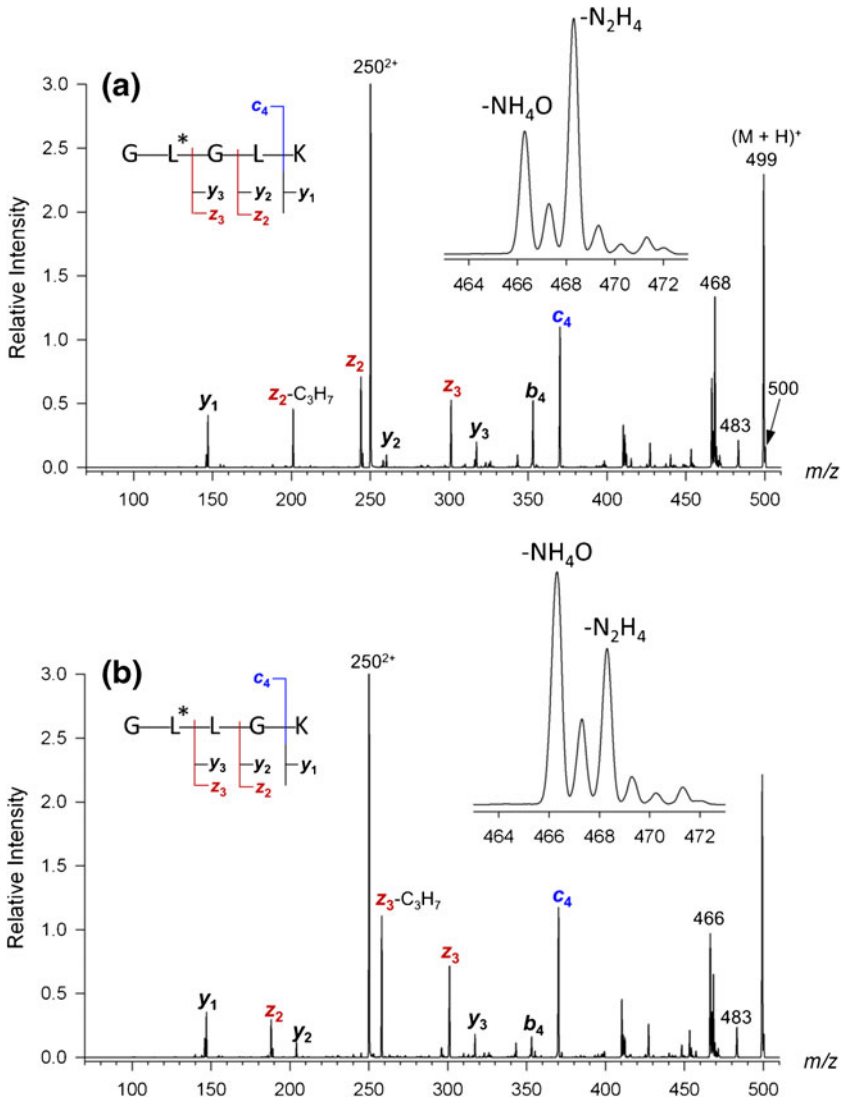

Figure 2. Electron transfer dissociation mass spectra of **(a)** $(GL^*GLK + 2H)^{2+}$ and **(b)** $(GL^*LGK + 2H)^{2+}$

complexes of $(GL^*GLK+2CE+2H)^{2+}$ at *m/z* 514. The first sequence, shown in Figure 3a, b, and e, started with ETD-MS^2 of the mass-selected *m/z* 514 ion resulting in a major loss of neutral CE to give a singly charged fragment ion of $(GL^*GLK+CE+2H)^{+\cdot}$ at *m/z* 764.4647 (theor. *m/z* 764.4638, Figure 3a). CID-MS^3 of mass-selected *m/z* 764 provided the $(GL^*GLK+2H)^{+\cdot}$ cation-radical at *m/z* 500.3076 as virtually the only product (Figure 3b). Further CID-MS^4 of the long-lived *m/z* 500 cation-radical resulted in dominant losses of N_2H_x and $[NH_4O]$ giving the *m/z* 466–471 fragment ions, but no sequence ***c*** and ***z*** ions (Figure 3e). The alternative reaction sequence (Figure 3c, d, e) started with CID-MS^2 of the mass-selected *m/z* 514 ion resulting in the loss of a neutral CE molecule and forming the $(GL^*GLK + CE + 2H)^{2+}$ ion at *m/z* 382 (Figure 3c). ETD-MS^3 of mass selected *m/z* 382 dication cleanly gave the *m/z* 500 cation-radical by loss of a neutral CE molecule (Figure 3d). Finally, the CID-MS^4 spectrum of thus generated *m/z* 500 cation-radical was identical with that in Figure 3e, showing major losses of N_2H_4 and $[NH_4O]$.

The above-described results can be summarized as follows. Electron transfer to the diazirine containing dications triggers competing backbone N–C_α bond dissociations and rearrangements involving the diazirine ring. The rearrangements produce long-lived, charge-reduced, cation-radicals, which upon collisional activation undergo eliminations of small molecules and radicals. This indicates that the non-dissociating peptide cation-radicals have structures in which the ETD-like backbone dissociations are disfavored. The fact that secondary cation-radical fragments (*m/z* 468) prefer charge-driven backbone dissociations and not radical driven side-chain losses indicates that the unpaired electron is parked in a very stable radical site.

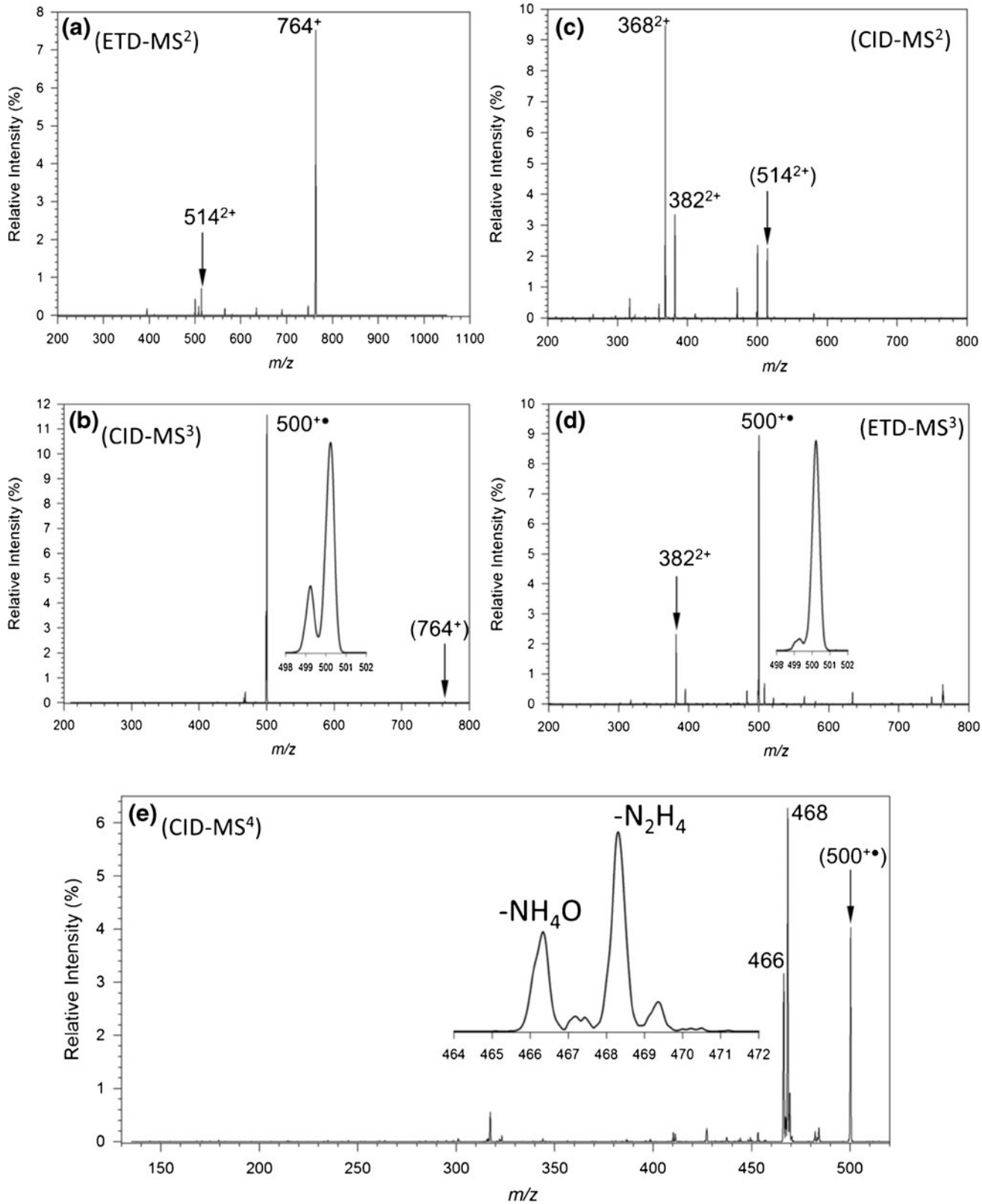

Figure 3. **(a)** ETD spectrum of $(GL^*GLK+2\ CE+2H)^{2+}$ at *m/z* 514. **(b)** CID spectrum of the *m/z* 764 fragment ion from **(a)**. **(c)** CID spectrum of $(GL^*GLK+2\ CE+2H)^{2+}$ at *m/z* 514. **(d)** ETD spectrum of the *m/z* 382 fragment ion from **c**. **(e)** CID spectrum of the *m/z* 500 fragment ion from **(b)** and **(d)**

Deuterium Exchange Measurements

To further characterize the unusual loss of N_2H_4 and [NH_4O], we carried out deuterium exchange experiments. The goal was to exchange in solution all nine labile protons in GL*GLK, GL*LGK, and GL*GGK peptides to a high degree of conversion and then deuterate the peptides by electrospray to produce D_{10} singly charged and D_{11} doubly charged ions as the main species. Under forcing conditions of H/D exchange described in the Experimental section we achieved mean degrees of deuteration [50] of α(D)=0.925 and 0.904, and 0.934 for GL*GLK, GL*LGK, and GL*GGK, respectively. Simple electrospray from a D_2O and CH_3OD solution of 99.5 % D quality but without forcing conditions gave α(D)=0.79 due to back exchange. Note that the latter α(D) gives only 9 % of D_{10} species, and the ion contains 52 % of the combined ^{13}C and ^{15}N isotopologues of the less deuterated ions. Our best enrichment gave the experimental distribution of deuterated doubly charged GL*GLK as 0.6 % D_7, 3.7 % D_8, 15.3 % D_9, 37.8 % D_{10}, and 42.4 % D_{11} which agreed with a statistical binomial distribution based on α(D)=0.925 within 0.4 % root-mean square deviation. In practical terms, the D_{11} ion contained <20 % of ^{13}C and ^{15}N isotopic contaminants. The enrichment was comparable for GL*GGK and slightly lower for doubly charged GL*LGK which gave 1.3 % D_7, 6.6 % D_8, 20.5 % D_9, 38.5 % D_{10}, and 32.8 % D_{11} with a correspondingly higher ($^{13}C+^{15}N$) contamination (25 %) of the D_{11} species. The ETD spectra of the D_{11} doubly charged ions from GL*GLK and GL*LGK are displayed in Supplemental Data Figure S6a, b, and that for GL*GGK in Supplemental Data Figure S7a. The backbone fragments showed the expected mass shifts due to the presence of exchangeable deuterium atoms, e.g., +6 for $\boldsymbol{y_1}$ at *m/z* 153, +5 for $\boldsymbol{z_2}$ at *m/z* 249, +6 for $\boldsymbol{z_3}$ at *m/z* 307, and +8 for $\boldsymbol{c_4}$ at *m/z* 378 for GL*GLK and +5 for $\boldsymbol{z_2}$ at *m/z* 193 in GL*LGK. The ETD spectra of the deuterated peptides showed abundant charge-reduced cation-radicals at *m/z* 511 (Figure S6a, b) and *m/z* 455 (Figure S7a), which were largely free of $^{13}C+^{15}N$ isotope contaminants. The group of fragment ions due to $N_2(H,D)_x$ and $N(H,D)_4O$ losses showed clusters of peaks at *m/z* 473–479 with relative intensities that differed for GL*GLK and GL*LGK. The clusters were made of fragment ions due to losses of $N_2(H,D)_3$, $N_2(H,D)_4$, [$N_2(H,D)_5$], and [$N(H,D)_4O$] neutrals that overlapped at several *m/z* values. Exact deconvolution of the individual ion intensities was not possible on the basis of the low-resolution mass spectra because the system of 7–8 linear equations that described the overlaps contains 16 variables and therefore was underdetermined. However, reasonably tight fits for the main components were obtained (Supplementary Data Figure S8a, b) with parameters given in Table 1. These indicated that the major neutral fragments, [NH_4O] and N_2H_4, predominantly incorporated three and four deuterium atoms with minor involvement of species having two light hydrogen atoms.

Table 1. Relative Abundances of Neutral Fragment Isotopologues from ETD of GL*GLK and GL*LGK D_{11} Dications

	%Loss of D_x neutral species									
	GL*GLK					GL*LGK				
Fragment	D_1	D_2	D_3	D_4	D_5	D_1	D_2	D_3	D_4	D_5
$N_2(H,D)_3$		37	34	29			37	34	29	
$N_2(H,D)_4$		10	40	50			10	40	50	
$N_2(H,D)_5$	3	10	10	52	25	3	10	10	47	30
$N(H,D)_4O$	5	8	52	35		2	8	48	42	

The charge-reduced $(GL*GGK\text{-}d_9+2D)^{+\cdot}$ ion at *m/z* 455 was mass-selected and submitted to CID-MS^3. The resulting mass spectrum (Figure S7b) showed a dominant loss of $N_2(H,D)_4$ and [$N(H,D)_4O$] at *m/z* 417–421, but virtually no backbone sequence fragment ions. Note that the charge-reduced ions were free of ^{13}C and ^{15}N isotope satellites and had lifetimes of >200 ms before being subjected to CID. The dominant $N_2(H,D)_4$ and [$N(H,D)_4O$] losses are quite analogous to those from ions generated from crown-ether complexes and indicate that the long-lived ions underwent rearrangements induced by the electron attachment.

Discussion

The experimental results indicated two major processes induced by electron attachment to the diazirine-containing peptide ions. One type is standard N–C_α backbone dissociations yielding sequence fragment ions. These proceed in the peptides under study regardless of the presence of the diazirine ring and produce similar $\boldsymbol{c}$ and $\boldsymbol{z}$ ion relative intensities (Figure 1). The other processes involve eliminations of neutral fragments of comprehensive elemental composition N_2H_4, [N_2H_5], and [NH_4O]. Out of these, [N_2H_5] and [NH_4O] are extremely weakly bound hypervalent radicals that are unlikely to be formed in the course of peptide cation-radical dissociations. Table S1 (Supplementary Data) summarizes the energetics of [N_2H_5] and [NH_4O] dissociations and illustrates that the formation of these species is substantially endothermic. The loss of [NH_4O] likely occurs in two steps (e.g., as consecutive eliminations of NH_3 and OH or H_2O and NH_2), which are consistent with the incorporation of four deuterium atoms from the peptide exchangeable positions. The D_3H species can arise by radical-driven hydrogen atom transfer from a nonexchangeable position. Eliminations of [NH_4O] as NH_2OH+H or NH_2O+H_2 would presumably favor loss of three deuterium atoms in the neutral fragments. Neutral energetics favors ($NH_2^\bullet + H_2O$) of ΔH_f=−53 kJ mol^{-1} over ($NH_3 + OH^\bullet$) of ΔH_f=−7 kJ mol^{-1} [51]. However, the uncertainty as to the nature of the neutral species precludes discussion of the dissociation mechanisms. We note that the *m/z* 466 ion formed by [NH_4O] elimination does not undergo loss of N_2 on CID-MS^3, which is otherwise a dominant dissociation of diazirine-containing even-electron

peptide ions of this type. Hence, it appears that the diazirine ring in the *m/z* 466 ion has undergone a rearrangement upon electron attachment. Further, loss of [NH_4O] occurs also in ETD of GL*GGK-NH_2 and GL*GGKK-NH_2 (Figure S2) and, hence, does not require a free carboxyl group.

The N_2H_4 neutral fragment is most likely a hydrazine molecule originating from a rearranged diazirine ring. Alternative eliminations of two NH_2 radicals or ammonia and nitrene (NH) are substantially more energy-demanding, as indicated by the neutral enthalpies of formation, ΔH_f=95, 331, and 378 kJ mol^{-1} for hydrazine, (NH_3+NH), and $2NH_2^{\bullet}$, respectively [51]. Neutral hydrazine is a strong base in the gas phase (PA=854 kJ mol^{-1}, close to that of ammonia) [51] that can undergo H/D exchange in an ion–molecule complex with the peptide fragment ion. The H/D content in the neutral hydrazine molecule (Table 1) can be due to an elimination reaction involving both the exchangeable D and nonexchangeable H atoms, followed by H/D exchange with the remaining peptide exchangeable D (Scheme 1). Considering a statistical exchange unbiased by kinetic isotope or other effects, a close fit with the Table 1 data was obtained for an initially formed $N_2D_2H_2$ undergoing H/D exchange with the nine remaining exchangeable peptide D atoms that gave 46 % D_4, 46 % D_3, and 8 % D_2 in the hydrazine molecules to be eliminated. The fit can be further improved to within 2 % root-mean square deviation by considering an initial elimination of 46 % $N_2H_2D_2$, 31 % N_2HD_3, 15 % N_2H_3D, and 8 % N_2H_4 followed by H/D exchange. Regardless of the fitting details, the data unambiguously show that both exchangeable and nonexchangeable hydrogen atoms are involved in the hydrazine molecule elimination.

The fragment ion thus formed (*m/z* 468) has a system of conjugated double bonds at the N-terminal residues that is expected to stabilize the radical in a captodative electronic structure [52]. This is consistent with the lack of radical-induced fragmentations in CID of the *m/z* 468 ion from GL*GLK, which forms mainly b_4, b_3, y_4, and y_1 ions upon CID. CID of the *m/z* 468 ion from GL*LGK shows a competition between the very facile radical induced elimination of C_4H_8 from the Leu side-chain [47] and the backbone amide cleavages. A conspicuous feature of the backbone cleavages is their frequency and competition for proton between the complementary *b* and *y* fragments. For example, backbone amide cleavages in the *m/z* 468 ion from GL*GLK are observed to occur between the G-L*, G-L, and L-K residues, but not between the L*-G ones. The b_4 and y_1 fragments compete for the charging proton and appear as the corresponding ions in the CID spectra, whereas the b_3 fragment ion is not accompanied by the complementary y_2 ion. This is unusual, because the peptide basicity typically correlates with the number of amino acid residues of the same type. Thus, contrary to the experimental data, a y_2 fragment would be expected to be more basic than y_1 to compete for a proton with the b_3 fragment, which in turn would be expected to be less basic than b_4. We argue that the backbone dissociations can be interpreted by the structure of the *m/z* 468 ion and its homologues from GL*GGK and GL*GGK-NH_2 that display a quite analogous behavior. Scheme S1 (Supplementary Data) shows the presumed mechanism for the formation of the b_3 fragment ion, when proceeding by the standard oxazolone pathway [53]. The oxazolone ring in the b_3 ion is conjugated with the unsaturated system of the GL* residues, which is expected to increase basicity and prevent proton transfer to the complementary GK $\boldsymbol{y_2}$ fragment. To examine this assumption, we calculated the free energy for the proton transfer from the b_3 ion to the GK neutral forming the b_3 neutral and $\boldsymbol{y_2}$ ion fragments from GL*GGK. The B3-PMP2 and M06-2X calculated ΔG_T values differed in that the former favored protonation of the $\boldsymbol{b_3}$ whereas the latter favored protonation of the $\boldsymbol{y_2}$ fragments (Figure S9, Supplementary Data). The B3-PMP2 data are in full agreement with preferential $\boldsymbol{b_3}$ protonation and absence of the complementary $\boldsymbol{y_2}$ ion in the CID spectrum. Both sets of data indicate that the formation of the $\boldsymbol{b_3}$ ion is favored at higher temperatures pertinent to CID, due to the negative protonation entropy of the conformationally flexible GK peptide. It may be noted that the calculated GB values for GK (943–963 kJ mol^{-1}, Table 2) fall within a range that is compatible with the GB reported on the basis of earlier approximate measurements (GB=934–953 kJ mol^{-1}) [54]. A conspicuous feature of the b_3 ion is that it is a conjugated enolamine cation-radical rather than a standard protonated oxazolone (Supplemental Data Scheme S1). In contrast, amide cleavage next to the Lys residue presumably generates a standard oxazolone-protonated b_4 fragment which competes for proton with the

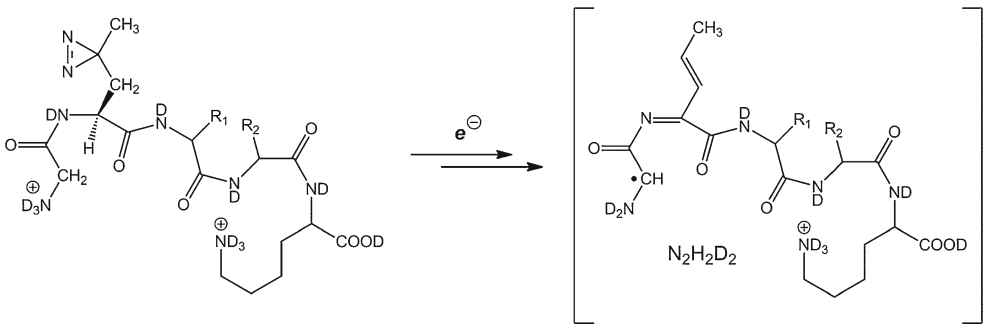

Scheme **1.**

Table 2. Relative Energies

Species/reaction	Relative Energy[ab]					
	B3LYP 6-31+G(d,p)	M06-2X	B3LYP 6-311++G(2d,p)	MP2	B3-MP2	M06-2X
$\boldsymbol{b_3}^+ \rightarrow \boldsymbol{b_3} + H^+$	991	975	989	973	981(988)[c](951)[d]	971(980)[c](943)[d]
$(GK+H)^+ \rightarrow GK + H^+$	1008	1009	1004	1007	1005(1011)[c](943)[d]	1003(1009)[c](963)[d]
$\mathbf{1}^{2+} \rightarrow \mathbf{1}^{+\bullet}$	576 (5.97)[e]	572 (5.92)[e]	575 (5.96)[e]	427 (4.43)[e]	501 (5.19)[e]	572 (5.93)[e]
$\mathbf{1}^{2+} \rightarrow \mathbf{1}^{+\bullet}$ (VN)[f]			523	402	463	482
$\mathbf{1}^{+\bullet} \rightarrow \mathbf{2}^{+\bullet}$	−162	−138	−165	−256	−211	−142
$\mathbf{1}^{+\bullet} \rightarrow \mathbf{3}^{+\bullet}$	−160	−133	−167			−140
$\mathbf{1}^{+\bullet} \rightarrow \mathbf{4}^{+\bullet}$	−238	−188	−250	−309	−280	−200
$\mathbf{1}^{+\bullet} \rightarrow \mathbf{5}^{+\bullet} + N_2H_4$	−130	−35	−148	−155	−151	−53
$(\mathbf{6} + H)^+ \rightarrow \mathbf{6} + H^+$	1094	1103	1089	1100	1094	1098
$7^{-\bullet} \rightarrow \mathbf{6} + e^-$	129 (1.34)[e]	148 (1.54)[e]	124 (1.29)[e]	135 (1.40)[e]	130 (1.34)[e]	144 (1.50)[e]
$\mathbf{8}^{\bullet} \rightarrow 7^{-\bullet} + H^+$	1241	1300	1237	1253	1245	
$\mathbf{8}^{\bullet} \rightarrow (\mathbf{6} + H)^+ + e^-$	276 (2.86)[e]	346(3.58)[e]	272 (2.82)[e]	278 (2.88)[e]	274 (2.85)[e]	
$\mathbf{9}^{+\bullet} \rightarrow 8^{\bullet} + H^+$	1119	1041	1122	1064	1093	

[a]In kJ mol^{-1}
[b]Including B3LYP or M06-2X/6-61+G(d,p) zero-point energy corrections
[c]298K enthalpies
[d]298 K free energies
[e]Energies in electron volts
[f]Vertical transition

Lys $\boldsymbol{y_1}$ fragment. One can also presume that the C_α radical and the conjugated system in the *m/z* 468 ion lower the nucleophilicity of the N-terminal Gly amide oxygen and, thus, hamper its participation in the formation of the b_2 ion, which is not observed in the CID spectrum.

Precursor Ion Structures

The nature of the diazirine ring rearrangement was investigated by obtaining structures of potential intermediates formed by electron attachment to $(GL^*GGK + 2H)^{2+}$. As ion conformations may play a role in these rearrangements, we first investigated precursor ion structures. The common force-fields used in conformational searches do not include parameters for the diazirine ring; therefore we investigated the effect that substituting photo leucine for the common Leu residue had on the major interactions affecting the gas-phase ion conformations. Exhaustive conformational search [33] was carried out for $(GLGGK + 2H)^{2+}$ and $(GLGGK\text{-}NH_2+H)^+$ and the conformers were ranked according to their free energies. Then, the Leu residues in selected low-energy conformers were converted into photo Leu (L*), and the $(GL^*GGK + 2H)^{2+}$ and $(GL^*GGK\text{-}NH_2+H)^+$ ions were fully optimized with B3LYP and M06-2X. Figure S10 (Supplementary Data) shows that the ranking of conformer energies did not change upon L*/Leu substitution. This result is significant because it indicates that the photo-Leu residue does not disrupt hydrogen bonding interactions that mainly affect the ion conformation. Hence, one can perform an exhaustive conformational search with peptides containing the conventional Leu residue and then simply modify the low-energy conformers by converting L to L*.

Cation-Radicals

Electron attachment to $(GL^*GGK + 2H)^{2+}$ ($\mathbf{1}^{2+}$) was first investigated as a vertical process to assess the available electronic states in the cation-radical ($\mathbf{1}^{+\bullet}$). The vertical recombination energies were calculated as RE_v=4.80 and 4.99 eV by B3-PMP2 and M06-2X, respectively (Table 2). Figure S11 (Supplementary Data) shows the manifold of low-lying electronic states in vertically formed $\mathbf{1}^{+\bullet}$. Both B3LYP and M06-2X/6-311++G(2d,p) wave functions show substantial delocalization of electron density by mixing of the N-terminal ammonium 3 s Rydberg, amide π*, and diazirine π* orbitals of the N=N double bond. Full geometry optimization of $\mathbf{1}^{+\bullet}$ produced a zwitterionic cation-radical as the ground electronic state that included an N-terminal Gly amide anion-radical and the protonated Lys and N-terminal ammonium groups (Scheme 2).

The adiabatic recombination energy of $\mathbf{1}^{+\bullet}$ was RE_{adiab}= 5.19 and 5.93 eV by B3-PMP2 and M06-2X, respectively (Table 2). The zwitterionic character of $\mathbf{1}^{+\bullet}$ was substantiated by an elongated amide C–O bond (1.308 Å), pyramidization at the amide carbon, and the calculated unpaired electron densities. Those showed major accumulation of spin density in the N-terminal Gly amide (70 % and 89 % by B3LYP and M06-2X, respectively). However, there was non-negligible spin density at the diazirine nitrogen atoms (22 % and 15 % by B3LYP and M06-2X, respectively) that indicated that the π* electronic system of the diazirine ring was capable of interaction with the amide π* system. This notion was further investigated by TD-DFT calculations of low excited states from vertical excitation of relaxed $\mathbf{1}^{+\bullet}$. Both the B3LYP and M06-2X wave functions (Figure S12, Supplementary Data) clearly indicated there were interactions between the diazirine π* electronic system and the

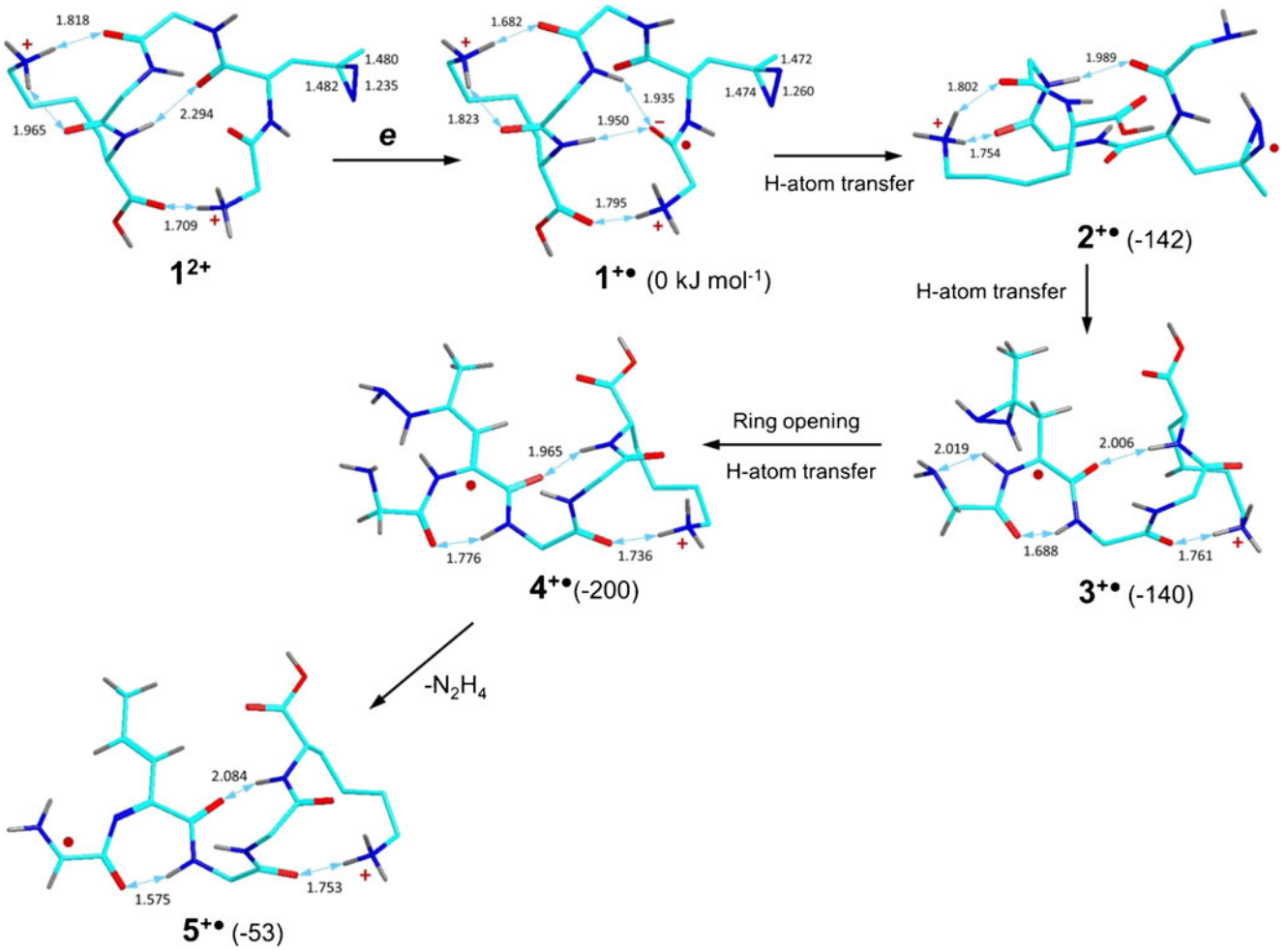

Scheme **2.**

ammonium 3 s Rydbergs in the A and B states from M06-2X and the C state from B3LYP. These interactions further indicated that the diazirine moiety could have a finite electron affinity.

The intrinsic electron affinity of gaseous diazirine has not been reported in the literature, although electron paramagnetic resonance spectra of simple diazirines indicated that stable anion-radicals were formed by electrochemical reduction in acetonitrile solution [55]. To circumvent excited-state calculations with the dications, we examined electron attachment to neutral GL*GGK-NH_2 (6, Figure S13) where the diazirine group was the only potential electron acceptor. Vertical electron attachment to GL*GGK-NH_2 gave anion-radical energies that were above that of the neutral molecule, indicating negative electron affinities and no bound states in the anion. However, full geometry optimization of the anion-radicals resulted in a substantial lowering of potential energy to give strongly bound states ($7^{-\cdot}$, Figure S13) and adiabatic electron affinities of EA_{adiab}=1.34 and 1.53 eV from the respective B3-PMP2 and M06-2X single point energies and including zero-point corrections (Table 2). The bound anion-radical, $[GL^*GGK\text{-}NH_2]^{-\cdot}$ ($7^{-\cdot}$) showed a substantial elongation of the diazirine N–N bond from 1.232 Å in the neutral molecule to 1.361 Å in the anion (Figure S13, Supplementary Data). The diazirine N=N stretching frequency dropped from ν_{sym}(N=N)=1674 cm^{-1} in **6** to 1481 cm^{-1} in $7^{-\cdot}$ indicating a lower force constant for this bond in the anion-radical. These structural features and the calculated spin densities demonstrated that the electron was attached to the N=N π* orbital of the diazirine ring. The effect of a remote charge on the electron attachment to the diazirine ring was investigated with $(GL^*GGK\text{-}NH_2+H)^{+-}$ (**8**$^{\bullet}$) generated by Lys protonation of the diazirine-based anion-radical. The zwitterionic species (**8**$^{\bullet}$, Figure S13) retained the unpaired electron in the diazirine ring whereas the proton was confined in the Lys NH_3 group and protected by internal solvation by the neighboring Gly amide carbonyl. The electron affinity of the diazirine ring in the zwitterion was 2.6 eV, a notable increase compared with the neutral amide due to the Coulomb effect of the charged Lys residue. Further protonation at the N-terminal Gly in the $(GL^*GGK\text{-}NH_2+H)^{+-}$ zwitterion resulted in a spontaneous proton transfer to the diazirine ring to give a Lys-protonated diazirine-radical (**9**$^{+\cdot}$, Figure S13).

Crown-Ether Effects

The electronic properties of the diazirine ring, as revealed by quantum chemistry calculations, gave a clue to the behavior of the peptide-ion crown-ether (CE) complexes upon ETD (Figure 3). Complexation with CE of primary ammonium groups results in a substantial lowering of intrinsic recombination energies in the complexes (e.g., from 4.0–4.2 eV in alkylammonium ions [56] to 1.7–2.0 eV in CE complexes [57, 58]. This effect is due to the substantial stabilization of the charged ammonium group by hydrogen bonding to the CE oxygens, which is perturbed by electron attachment forming the radical [58]. The other effect of CE coordination is that it disrupts H-bonding of the ammonium groups to the peptide amide carbonyls and thus changes the precursor ion conformation [49].

The combined effect of conformational change and electronic perturbation dramatically affects the ordering of electronic state energies in the diazirine-containing peptide–CE complexes. Owing to the lack of internal solvation, the CE-coordinated ammonium groups move away from the peptide backbone, decreasing the Coulomb stabilization of the amide π* state (***X***, Figure S12) in the charge-reduced cation-radical. Thus, the energy level for this state goes up. The intrinsic electronic properties of the diazirine ring presumably are not much affected by the Lys-NH_3-crown complexation, and the change of ion conformation results in a small decrease of the diazirine recombination energy because of diminished Coulomb stabilization. These shifts in the *X* and *A*, *B* state energies (Supplemental Data Figure S12) can lead to a reversal of the energy levels making the diazirine ring the preferred electron attachment site. This would explain the dramatically changed chemistry following electron attachment to peptide–CE complexes that showed exclusively diazirine-based radical dissociations (Figure 2e).

Franck-Condon Effects on Electron Transfer

The electron affinity calculations also indicated that electron attachment to both the N-terminal Gly amide and the diazirine ring in $(GLGGK + 2H)^{2+}$faced substantial Franck-Condon effects because of the differences in the equilibrium structures of the neutral and reduced groups. Regarding the amide, the Franck-Condon effect can be judged by the difference between the adiabatic recombination energy, RE_{adiab}=5.19 eV, and the vertical value, RE_v= 4.75 eV, both from B3-PMP2/6-311++G(2d,p) energies (Table 2). The M06-2X energies gave an even greater difference, RE_{adiab}=5.93 eV and RE_v=4.99 eV. Large $RE_{adiab} - RE_v$ difference was also obtained for the diazirine ring in GL*GGK-NH_2, where it ranged from 1.25 to 1.63 eV. The Franck-Condon effects may affect the competition between the backbone and diazirine dissociations following electron transfer. In the current model, the electron is presumed to non-adiabatically cross from an initial Rydberg state to the electronic state of the group to undergo dissociation. The crossing frequency depends on the coupling term (H_{12}) between the potential energy surfaces and the vibrational frequencies of the involved bonds [59]. The diazirine ring in $\mathbf{1}^{2+}$ has the following stretching vibrational frequencies: ν_{sym}(C–N)=708 cm^{-1}, ν_{asym}(C–N)=787 cm^{-1}, and ν(N=N)=1674 cm^{-1}. Remarkably, these occur in the same regions as the out-of-plane amide N-H (478–697 cm^{-1}) and N-C-O vibrations (709–795 cm^{-1}), and the amide C=O stretching vibrations (1671–1701 cm^{-1}) that have to be excited in surface crossing. These data indicate that the crossing frequencies can be comparable, consistent with the ETD spectra that show ca. 4:1 ratios of c+z backbone to diazirine fragment ion intensities.

Electron attachment to the diazirine ring is expected to trigger a highly exothermic proton transfer forming a hydrazinyl-radical. Likewise, the diazirine ring has a substantial hydrogen atom affinity, as evidenced by the exothermic H-atom transfer in $\mathbf{1}^{+\cdot}$ forming the hydrazinyl-radical $\mathbf{2}^{+\cdot}$ (Scheme 2), which is accompanied by an energy change of ΔH_{rxn}=−142 kJ mol^{-1} from the M06-2X/6-311++G(2d,p) energies (Table 2). Note that the $\mathbf{1}^{+\cdot} \rightarrow \mathbf{2}^{+\cdot}$ isomerization involves an exchangeable proton regardless of whether it proceeds as an H-atom migration to the neutral diazirine in the ground electronic state or as a proton migration to the diazirine anion-radical in a low-lying excited state. Radical $\mathbf{2}^{+\cdot}$ can undergo several isomerization pathways including hydrogen atom and proton transfers combined with diazirine ring opening on the way to eliminate hydrazine. An exhaustive investigation of these pathways would be beyond the scope of this work. We note that the hydrogen transfers and ring-opening isomerizations, as well as the elimination of hydrazine, are all exothermic reactions (Table 2) as documented by the relative energies of intermediates $\mathbf{3}^{+\cdot}$, $\mathbf{4}^{+\cdot}$, and the fragment ion $\mathbf{5}^{+\cdot}$ (Scheme 2).

Diazirine as a Disruptor of Backbone Cleavages

The electronic properties of the diazirine ring place it in the group of substituents disrupting backbone fragmentations of peptide ions upon ExD [11–14]. A previous study by Sohn et al. used peptides furnished with benzyl substituents carrying electron withdrawing groups (EWG=3-NO_2, 3,5-NO_2, 3-CN, 3,5-CN, and 1,2,3,4,5-F_5), of which the nitro and cyano substituents showed major effects on quenching peptide backbone dissociations [14]. Sohn et al. concluded, on the basis of a comparison of the substituents' electron affinities, that a disrupting effect can be expected for groups having electron affinities >1 eV to sequester the unpaired electron in their π* systems [14]. A related paper analyzed hydrogen atom transfer to substituted benzyl groups and concluded that the NO_2 and CN groups had large H-atom affinities and very low transition state energies for H atom migration so they functioned as hydrogen atom traps, quenching radical-driven backbone dissociations [12]. The diazirine ring shows both these kinds of properties by having

a substantial intrinsic electron (1.5 eV) and hydrogen atom affinity (142–211 kJ mol^{-1}). However, the disruptive effect of the diazirine ring is only moderate, as the dissociations involving the diazirine moiety amount to 18 %–21 % of ETD fragments but do not quench the backbone fragmentations. The moderate effect of the diazirine ring is also favorable for the future use of ETD for sequencing photolabeled peptides and their photochemical products.

Acknowledgments

Financial support by a grant to F.T. from the National Science Foundation (CHE-1055132) is gratefully acknowledged. K.L. thanks the ARCS foundation for financial support. Instrumentation support for the low-resolution ETD mass spectra measurements was provided by the University of Washington Proteomics Resource (Dr. Priska von Haller). The authors thank Drs. Rob Moritz and Sarah Lee of the Seattle Institute for Systems Biology for providing access to the Thermo-Fisher Orbitrap Velos ETD instrument, and Dr. Jan Urban for advice with peptide syntheses.

References

1. Li, X., Cournoyer, J.J., Lin, C., O'Connor, P.B.: The effect of fixed charge modifications on electron capture dissociation. *J. Am. Soc. Mass Spectrom.* **19**, 1514–1526 (2008)
2. Chamot-Rooke, J., van der Rest, G., Dalleu, A., Bay, S., Lemoine, J.: The combination of electron capture dissociation and fixed charge derivatization increases sequence coverage for O-glycosylated and O-phosphorylated peptides. *J. Am. Soc. Mass Spectrom.* **18**, 1405–1413 (2007)
3. Chung, T.W., Tureček, F.: Selecting fixed-charge groups for electron-based peptide dissociations. A computational study of pyridinium tags. *Int. J. Mass Spectrom.* **276**, 127–135 (2008)
4. Chung, T.W., Tureček, F.: Electron transfer to charge-tagged peptide ions. A computational analysis of electronic states. *Eur. J. Mass Spectrom.* **14**, 367–378 (2008)
5. Chung, T.W., Moss, C.L., Zimnicka, M., Johnson, R.S., Moritz, R.L., Tureček, F.: Electron capture and transfer of peptides tagged with tunable fixed-charge groups. Structures and dissociation energies. *J. Am. Soc. Mass Spectrom.* **22**, 13–30 (2011)
6. Zimnicka, M., Moss, C.L., Chung, T.W., Hui, R., Tureček, F.: Tunable charge tags for electron-based methods of peptide sequencing. design and applications. *J. Am. Soc. Mass Spectrom* **23**, 608–620 (2012)
7. Ross, P.L., Huang, Y.L.N., Marchese, J.N., Williamson, B., Parker, K., Hattan, S., Khainovski, N., Pillai, S., Dey, S., Daniels, S., Purkayastha, S., Juhasz, P., Martin, S., Bartlet-Jones, M., He, F., Jacobson, A., Pappin, D.J.: Multiplexed protein quantitation in *Saccharomyces cerevisiae* using amine-reactive isobaric tagging reagents. *Mol. Cell. Proteomics* **3**, 1154–1169 (2004)
8. Han, H., Pappin, D.J., Ross, P.L., McLuckey, S.A.: Electron transfer dissociation of iTRAQ labeled peptide ions. *J. Proteome Res.* **7**, 3643–3648 (2008)
9. Hennrich, M.L., Boersema, P.J., van den Toorn, H., Mischerikow, N., Heck, A.J.R., Mohammed, S.: Effect of chemical modifications on peptide fragmentation behavior upon electron transfer induced dissociation. *Anal. Chem.* **81**, 7814–7822 (2009)
10. Jensen, C.S., Holm, A.I.S., Zettergren, H., Overgaard, J.B., Hvelplund, P., Nielsen, S.B.: On the charge partitioning between c and z fragments formed after electron-capture induced dissociation of charge-tagged lys-lys and ala-lys dipeptide dications. *J. Am. Soc. Mass Spectrom.* **20**, 1881–1889 (2009)
11. Belyayev, M.A., Cournoyer, J.J., Lin, C., O'Connor, P.B.: The effect of radical trap moieties on electron capture dissociation spectra of substance P. *J. Am. Soc. Mass Spectrom.* **17**, 1428–1436 (2006)
12. Tureček, F.: Electron predators are hydrogen atom traps. Effects of aryl groups on N–C_α bond dissociations of peptide radicals. *J. Mass Spectrom.* **45**, 1280–1290 (2010)
13. Jones, J.W., Sasaki, T., Goodlett, D.R., Tureček, F.: Electron capture in spin-trap capped peptides. An experimental example of ergodic dissociation in peptide cation-radicals. *J. Am. Soc. Mass Spectrom.* **18**, 432–444 (2007)
14. Sohn, C.H., Chung, C.K., Yin, S., Ramachandran, P., Loo, J.A., Beauchamp, J.L.: Probing the mechanism of electron capture and electron transfer dissociation using tags with variable electron affinity. *J. Am. Chem. Soc.* **131**, 5444–5459 (2009)
15. Ben Hamidane, H., Vorobyev, A., Larregola, M., Lukaszuk, A., Tourwe, D., Lavielle, S., Karoyan, P., Tsybin, Y.O.: Radical stability directs electron capture and transfer dissociation of β-amino acids in peptides. *Chem. Eur. J.* **16**, 4612–4622 (2010)
16. Sargaeva, N.P., Lin, C., O'Connor, P.B.: Unusual fragmentation of β-linked peptides by ExD tandem mass spectrometry. *J. Am. Soc. Mass Spectrom.* **22**, 480–491 (2011)
17. Kjeldsen, F., Zubarev, R.A.: Effects of peptide backbone amide-to-ester bond substitution on the cleavage frequency in electron capture dissociation and collision-activated dissociation. *J. Am. Soc. Mass Spectrom.* **22**, 1441–1452 (2011)
18. Hansen, T.A., Jung, H.R., Kjeldsen, F.: Electron transfer dissociation reveals changes in the cleavage frequencies of backbone bonds distant to amide-to-ester substitutions in polypeptides. *J. Am. Soc. Mass Spectrom.* **22**, 1953–1957 (2011)
19. Zimnicka, M., Chung, T.W., Moss, C.L., Tureček, F.: Perturbing peptide cation-radical electronic states by thioxoamide groups: Formation, dissociations and energetics of thioxopeptide cation-radicals. *J. Phys. Chem. A* **117***, 1265–1280 (2013)*
20. Kumar, A.B., Anderson, J.M., Manetsch, R.: Design, synthesis, and photoactivation studies of fluorous photolabels. *Org. Biomol. Chem.* **9**, 6284–6292 (2011)
21. Hashimoto, M., Hatanaka, Y.: Recent progress in diazirine-based photoaffinity labeling. *Eur. J. Org. Chem.* 2513–2523. doi:10.1002/ejoc.200701069 (2008)
22. Das, J.: Aliphatic diazirines as photoaffinity probes for proteins: Recent developments. *Chem. Rev.* **111**, 4405–4417 (2011)
23. Dubinsky, L., Bastiaan, P., Krom, B.P., Meijler, M.M.: Diazirine based photoaffinity labeling. *Bioorg. Med. Chem.* **20**, 554–570 (2012)
24. Liu, M.T.H.: Chemistry of Diazirines; Vol. I and II. CRC Press, Boca Raton (1987)
25. Korneev, S.M.: Valence Isomerization between diazo compounds and diazirines. *Eur. J. Org. Chem.* 6153–6175. doi:10.1002/ejoc.201100224 (2011)
26. Barton, D.H.R., Jaszberenyi, J.C., Theodorakis, E.A., Reibenspies, J.H.: The invention of radical reactions. 30. Diazirines as carbon radical traps. Mechanistic aspects and synthetic applications of a novel and efficient amination process. *J. Am. Chem. Soc.* **115**, 8050–8059 (1993)
27. Moss, R.A., Xue, S., Liu, W.: Mechanistic origins of acyloxydiazirines. *J. Am. Chem. Soc.* **116**, 10821–10822 (1994)
28. Moss, C.L., Chamot-Rooke, J., Brown, J., Campuzano, I., Richardson, K., Williams, J., Bush, M., Bythell, B., Paizs, B., Turecek, F.: Assigning structures to gas-phase peptide cations and cation-radicals. An infrared multiphoton dissociation, ion mobility, electron transfer and computational study of a histidine peptide ion. *J. Phys. Chem. B* **106**, 3445–3456 (2012)
29. Syka, J.E.P., Coon, J.J., Schroeder, M.J., Shabanowitz, J., Hunt, D.F.: Peptide and protein sequence analysis by electron transfer dissociation mass spectrometry. *Proc. Natl. Acad. Sci. U. S. A.* **101**, 9528–9533 (2004)
30. Janz, J.M., Ren, Y., Looby, R., Kazmi, M.A., Sachdev, P., Grunbeck, A., Haggis, L., Chinnapen, D., Lin, A.Y., Seibert, C., McMurry, T., Carlson, K.E., Muir, T.W., Hunt, S., Sakmar, T.P.: Direct interaction between an allosteric agonist pepducin and the chemokine receptor CXCR4. *J. Am. Chem. Soc.* **133**, 15878–15881 (2011)
31. Coste, J., LeNguyen, D., Castro, B.: PyBOP@: A new peptide coupling reagent devoid of toxic by-product. *Tetrahedron Lett.* **31**, 205–208 (1990)
32. Compton, P.D., Strukl, J.V., Bai, D.L., Shabanowitz, J., Hunt, D.F.: Optimization of electron transfer dissociation via informed selection of reagents and operating parameters. *Anal. Chem.* **84**, 1781–1785 (2012)
33. Moss, C.L., Chung, T.W., Wyer, J.A., Nielsen, S.B., Hvelplund, P., Tureček, F.: Dipole-guided electron capture causes abnormal dissociations of phosphorylated pentapeptides. *J. Am. Soc. Mass Spectrom.* **22**, 731–751 (2011)

34. Stewart, J.J.P.: Optimization of parameters for semiempirical methods. V. Modification of NDDO approximations and application to 70 elements. *J. Mol. Model.* **13**, 1173–1213 (2007)
35. Frisch, M.J., Trucks, G.W., Schlegel, H.B., Scuseria, G.E., Robb, M.A., Cheeseman, J.R., Scalmani, G., Barone, V., Mennucci, B., Petersson, G.A., Nakatsuji, H., Caricato, M., Li, X., Hratchian, H.P., Izmaylov, A.F., Bloino, J., Zheng, G., Sonnenberg, J.L., Hada, M., Ehara, M., Toyota, K., Fukuda, R., Hasegawa, J., Ishida, M., Nakajima, T., Honda, Y., Kitao, O., Nakai, H., Vreven, T., Montgomery Jr., J.A., Peralta, J.E., Ogliaro, F., Bearpark, M., Heyd, J.J., Brothers, E., Kudin, K.N., Staroverov, V.N., Kobayashi, R., Normand, J., Raghavachari, K., Rendell, A., Burant, J.C., Iyengar, S.S., Tomasi, J., Cossi, M., Rega, N., Millam, J.M., Klene, M., Knox, J.E., Cross, J.B., Bakken, V., Adamo, C., Jaramillo, J., Gomperts, R., Stratmann, R.E., Yazyev, O., Austin, A.J., Cammi, R., Pomelli, C., Ochterski, J.W., Martin, R.L., Morokuma, K., Zakrzewski, V.G., Voth, G.A., Salvador, P., Dannenberg, J.J., Dapprich, S., Daniels, A.D., Farkas, O., Foresman, J.B., Ortiz, J.V., Cioslowski, J., Fox, D.J.: Gaussian 09, Revision A.02. Gaussian, Inc, Wallingford (2009)
36. Becke, A.D.: New mixing of Hartree-Fock and local density-functional theories. *J. Chem. Phys.* **98**, 1372–1377 (1993)
37. Becke, A.D.: Density functional thermochemistry. III. The role of exact exchange. *J. Chem. Phys.* **98**, 5648–5652 (1993)
38. Zhao, Y., Truhlar, D.G.: The M06 suite of density functionals for main group thermochemistry, thermochemical kinetics, noncovalent interactions, excited states, and transition elements: Two new functionals and systematic testing of four M06-class functionals and 12 other functionals. *Theor. Chem. Accounts* **120**, 215–241 (2008)
39. Møller, C., Plesset, M.S.: A note on an approximation treatment for many-electron systems. *Phys. Rev.* **46**, 618–622 (1934)
40. Tureček, F., Wolken, J.K.: Dissociation energies and kinetics of aminopyrimidinium radicals by ab initio and density functional theory. *J. Phys. Chem. A* **103**, 1905–1912 (1999)
41. Wolken, J.K., Tureček, F.: Heterocyclic radicals in the gas phase. Experimental and computational study of 3-hydroxypyridinium radicals and cations. *J. Am. Chem. Soc.* **121**, 6010–6018 (1999)
42. Wolken, J.K., Tureček, F.: Modeling nucleobase radicals in the gas phase. Experimental and computational study of 2-hydroxypyridinium and 2-(1H)pyridone radicals. *J. Phys. Chem. A* **103**, 6268–6281 (1999)
43. Furche, F., Ahlrichs, A.: Adiabatic time-dependent density functional methods for excited state properties. *J. Chem. Phys.* **117**, 7433–7447 (2002)
44. Reed, A.E., Weinstock, R.B., Weinhold, F.: Natural population analysis. *J. Chem. Phys.* **83**, 735–746 (1985)
45. Liu, J., Liang, X., McLuckey, S.A.: On the value of knowing a z• ion for what it is. *J. Proteome Res.* **7**, 130–137 (2008)
46. Sun, Q., Nelson, H., Stolz, B.M., Julian, R.R.: Side chain chemistry mediates backbone fragmentation in hydrogen deficient peptide radicals. *J. Proteome Res.* **8**, 958–966 (2009)
47. Chung, T.W., Tureček, F.: Backbone and side-chain specific dissociations of *z* ions from non-tryptic peptides. *J. Am. Soc. Mass Spectrom.* **21**, 1279–1295 (2010)
48. Ledvina, A.R., Chung, T.W., Hui, R., Coon, J.J., Turecek, F.: Cascade dissociations of peptide cation-radicals. Part 2. Infrared multiphoton dissociation and mechanistic studies of z-ions from pentapeptides. *J. Am. Soc. Mass Spectrom.* **23**, 1351–1363 (2012)
49. Haag, N., Holm, A.I.S., Johansson, H.A.B., Zettergren, H., Schmidt, H.T., Nielsen, SB., Hvelplund, P., Cederquist, H.: Electron capture induced dissociation of doubly protonated pentapeptides: Dependence on molecular structure and charge separation. *J. Chem. Phys.* **134**, 035102/1–035102/6 (2011)
50. Tureček, F.: The use of labeled compounds. In: Splitter, J.S., Turecek, F. (eds.) Applications of Mass Spectrometry to Organic Stereochemistry, Appendix 1. VCH Publishers, New York (1994)
51. NIST Standard Reference Database Number 69, available at: http://webbook.nist.gov/chemistry/. Accessed 24 Mar 2013
52. Hopkinson, A.C.: Radical cations of amino acids and peptides: Structures and stabilities. *Mass Spectrom. Rev.* **28**, 655–671 (2009)
53. Yalcin, T., Khouw, C., Csizmadia, I.G., Peterson, M.R., Harrison, A.G.: Why are b ions stable species in peptide spectra? *J. Am. Soc. Mass Spectrom.* **6**, 1165–1174 (1995)
54. Harrison, A.G.: The gas-phase basicities and proton affinities of amino acids and peptides. *Mass Spectrom. Rev.* **16**, 201–217 (1997)
55. Elson, C.M., Liu, M.T.H., Mailer, C.E.S.R.: Studies of diazirine anion radicals. *J. Chem. Soc. Chem. Commun.* 504–506. doi:10.1039/C39860000504 (1986)
56. Yao, C., Turecek, F.: Hypervalent ammonium radicals. Competitive N–C and N–H bond dissociations in methylammonium and ethylammonium. *Phys. Chem. Chem. Phys.* **7**, 912–920 (2005)
57. Holm, A.I.S., Larsen, M.K., Panja, S., Hvelplund, P., Nielsen, S.B., Leib, R.D., Donald, W.A., Williams, E.R., Hao, C., Tureček, F.: Electron capture, femtosecond electron transfer and theory: A study of noncovalent crown ether 1, n-diammonium alkane complexes. *Int. J. Mass Spectrom.* **276**, 116–126 (2008)
58. Chung, T.W., Turecek, F.: Selecting fixed-charge groups for electron-based peptide dissociations. A computational study of pyridinium tags. *Int. J. Mass Spectrom.* **276**, 127–135 (2008)
59. Neff, D., Sobczyk, M., Simons, J.: Through-space and through-bond electron transfer within positively charged peptides in the gas phase. *Int. J. Mass Spectrom.* **276**, 91–101 (2008)